RSC Advances

COMMUNICATION

View Article Online
View Journal | View Issue

Photocatalytic degradation of methylene blue in ZIF-8

Huan-Ping Jing,[a] Chong-Chen Wang,*[ab] Yi-Wen Zhang,[b] Peng Wang[a] and Ran Li[a]

Cite this: *RSC Adv.*, 2014, **4**, 54454

Received 18th August 2014
Accepted 8th October 2014

DOI: 10.1039/c4ra08820d

www.rsc.org/advances

Metal–organic frameworks (MOFs), a new class of porous crystalline materials, have attracted great interest as a promising candidate for sustainable energy and environmental remediation. In this study, ZIF-8, a versatile MOF based on imidazolate ligands, was selected as a photocatalyst to decompose methylene blue (MB) under UV light irradiation. The influence factors, kinetics, and mechanism of photocatalytic MB degradation and stability of ZIF-8, were also studied. The results revealed that the ZIF-8 photocatalyst exhibited efficiently photocatalytic activity for MB degradation under UV irradiation, which was confirmed through the detection of hydroxyl radicals (˙OH) by a fluorescence method. The MB degradation over the ZIF-8 photocatalyst followed a pseudo-first-order kinetics model. ZIF-8 worked effectively over a wide pH range from 4.0 to 12.0, and showed both high adsorption capacity and degradation efficiency for MB in a strong alkaline environment. The enhanced efficiency in a strong alkaline environment resulted from the higher charged ZIF-8 ($pH > pH_{pzc}$) and the elevated yield of ˙OH facilitated by increased OH^- concentration. The possible pathway of photocatalytic degradation of MB in ZIF-8 was proposed. The results indicated that ZIF-8 can be used as a highly efficient photocatalyst to decompose organic pollutants.

1. Introduction

Metal–organic frameworks (MOFs), a new class of porous crystalline materials, have been of great interest due to their beneficial properties such as extremely high surface areas, well-ordered porous structures and structure designability,[1] which show them to be promising candidates for separation,[2–7] gas storage,[8–10] catalysts and photocatalysts,[10–14] carbon dioxide capture,[15,16] and so on.[2,3,17–21] Additionally, some MOFs, which can act as photocatalysts, are gave increasing attentions.[22–27] These emerging researches not only demonstrate porous MOFs materials to be a potential new class of photocatalysts for their catalytic degradation of organic pollutants under UV-visible irradiation, but also trigger extensive research on MOFs materials as photocatalysts. Compared to conventional semiconductor photocatalysts, the photoactive MOFs have some advantages in degrading organic pollutants: (i) the well-defined crystalline structures of MOFs are beneficial in the characterization and study of structure–property relationship of these solid photocatalysts; (ii) the modular nature of the MOFs synthesis allows the rational design and fine tuning of these catalysts at the molecular level, making the electronic structure of the MOFs catalysts to be easily tailored; (iii) the structural features of tunable active sites (*i.e.*, metal-oxoclusters and organic linkers) in MOFs lead to more efficiency of solar harnessing; (iv) different from typical TiO_2-based catalysts, the visible light photocatalytic activity can be easily introduced *via* the linker substitutions of organic chromophores in MOF structures, such as amino group.[22–27]

Methylene blue (MB) with molecular formula of $C_{16}H_{18}N_3SCl$ (FW 319.85 g mol^{-1}), is commonly used as a representative of widespread organic dyes that contaminate textile effluents and that are lowering light penetration, photosynthesis and damage the aesthetic nature of the water surface. The molecular structure of MB is illustrated in Scheme 1. Methylene blue (MB) is a heterocyclic aromatic chemical compound, which has many uses in a range of different fields, like biology and chemistry. At doses of 2–4 mg kg^{-1}, hemolytic anemia and skin

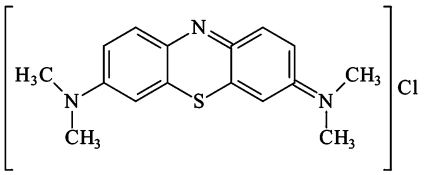

Scheme 1 Structure of methylene blue (MB).

[a]*Key Laboratory of Urban Stormwater System and Water Environment (Ministry of Education), Beijing University of Civil Engineering and Architecture, Beijing, 100044, China. E-mail: chongchenwang@126.com*

[b]*Beijing Engineering Research Center of Sustainable Urban Sewage System Construction and Risk Control, Beijing University of Civil Engineering and Architecture, Beijing, 100044, China*

desquamation may occur in infants. At doses of 7 mg kg^{-1}, nausea, vomiting, chest pain, fever, and hemolysis have been described. Hypotension may occur at doses of 20 mg kg^{-1}, and bluish discoloration of the skin can occur at 80 mg kg^{-1}.[28] There are currently numerous treatment processes for effluent discharged from industrial processes containing dyes, including biodegradation, chemical oxidation, flocculation, filtration, adsorption and photocatalysis.[28]

ZIF-8 [Zn(2-methylimidazole)$_2 \cdot 2H_2O$], a kind of MOF, is constructed from imidazolate organic ligands and Zn^{2+} center ions, which exhibits higher thermal and chemical stability than other MOFs.[29] It is its high BET specific surface area (SSA) ($\approx$2000 m^2 g^{-1})[30] and permanent porosity from its uniformly sized pore cavities (of $\approx$1.16 nm and pore volume of $\approx$0.60 cm^3 g^{-1})[30] that make ZIF-8 particularly desirable for many potential applications, such as gas storage,[31–35] separation by membrane sieving,[36–39] templating,[40,41] catalysis,[42–44] and shape-selective distillation,[45–48] sensing[49] and so on.[50,51]

With this paper, the ZIF-8 was synthesized and characterized by powder X-ray diffraction, Fourier transform infrared spectra FTIR, UV-vis diffuse reflectance spectra. And, ZIF-8 was selected as photocatalyst to decompose methylene blue (MB), a typical model of dye contaminant, under UV light irradiation. The influence factors (such as pH and initial MB concentration), kinetics and mechanism of photocatalytic MB degradation and stability of ZIF-8 were also studied. The results demonstrated that ZIF-8 is an excellent candidate for photocatalytic degradation of methylene blue (MB).

2. Experimental section

2.1. Materials

ZIF-8 [Zn(2-methylimidazole)$_2 \cdot 2H_2O$] was prepared by slow evaporation following the method as described by Chen *et al.*[52] A solution of 2-methylimidazole (0.2 mmol, 0.016 g) in methanol (5.0 mL) was slowly and carefully layered onto a solution of $Zn(OH)_2$ (0.1 mmol, 0.010 g) in aqueous ammonia (25%, 2.0 mL). Colorless polyhedral crystals began to appear after several days. After one month, they were collected, washed (methanol–water 1 : 1), and dried in air (yield 70%). 2-Methylimidazole, methanol, $Zn(OH)_2$, ammonia, methylene blue (MB), terephthalic acid, NaCl, HCl and NaOH were purchased from J&K Scientific Ltd. All reagents were analytical grade and used directly without further purification.

2.2. Characterization of ZIF-8

Powder X-ray diffraction (PXRD) patterns were recorded using Rigaku DMAX-IIIA diffractometer employing Cu Kα radiation. The Fourier transform infrared (FTIR) spectra were recorded from KBr pellets in the range of 4000–400 cm^{-1} on Nicolet 6700 spectrometer. UV-vis diffuse reflectance data were collected over the spectral range 200–1200 nm with Agilent Cary 5000 spectrophotometer equipped with an integrated sphere and $BaSO_4$ was used as a reference sample. The surface area, total pore volume and pore size distribution (PSD) of the samples were obtained from N_2 adsorption–desorption isotherms at 77 K using a Belsorp-mini instrument (BEL Japan Inc.). Before the sorption experiments, the samples were activated at 120 °C under vacuum (10^{-2} kPa) for 6 h. The method for determining the point of zero charge (pH_{pzc}) for ZIF-8 was modified by Wan Ngah *et al.*[53] The initial pH of 50 mL of 0.01 mol L^{-1} NaCl solution was adjusted to pH values ranging from 2.0–10.0 by adding either 0.1 mol L^{-1} HCl or 0.1 mol L^{-1} NaOH solution. A 0.15 g of ZIF-8 was added and the suspension was stirred for 48 h at 150 rpm. The pH_{pzc} was the point where the final pH (pH_{final}) and the initial pH ($pH_{initial}$) are equal.

2.3. Photocatalytic degradation

MB is commonly used as a representative of widespread organic dyes that are very difficult to decompose in waste streams under visible-light irradiation. Herein, the photocatalytic activities of ZIF-8 photocatalysts were evaluated by the photodegradation of MB dye under 500 W Hg lamp irradiation in open air, and under room temperature. The distance between the light source and the beaker containing reaction mixture was fixed at 5 cm. 25 mg of ZIF-8 photocatalyst was put into 50 mL of MB aqueous solution (10 mg L^{-1}) in a 50 mL flask. Prior to irradiation, the suspension was magnetically stirred in dark for 60 min to ensure the establishment of an adsorption–desorption equilibrium. During the photodegradation reaction, stirring was maintained to keep the mixture in suspension. One milliliter sample was extracted at regular intervals using 0.45 μm syringe filter (Shanghai Troody) for analysis.

2.4. Analytical methods of the photocatalytic process

A Laspec Alpha-1860 spectrometer was used to monitor the changes of the dye absorbance in the range of 400–800 nm in a 1 cm path length spectrometric quartz cell, and MB concentration was estimated by the absorbance at 664 nm. As widely accepted, hydroxyl radicals ($^{\bullet}OH$) have been deemed to be the crucial active species during the photocatalytic process. Usually, a high generation rate of $^{\bullet}OH$ results in rapid degradation and short reaction times to achieve specific treatment objectives. Terephthalic acid has the property to trap $^{\bullet}OH$ effectively and selectively, then produces 2-hydroxy terephthalic acid with a percent yield of 35%.[54] 2-Hydroxy terephthalic acid could emit fluorescence at 425 nm when excited at 315 nm. As a result, the yield of $^{\bullet}OH$ can be quantified by fluorescent measurement of the generated 2-Hydroxy terephthalic acid.[55] So, hydroxyl radical ($^{\bullet}OH$) mediated by ZIF-8 catalysts was detected by the fluorescence method using terephthalic acid as a probe molecule.[56] The experimental procedures were similar to those used in the measurement of above catalytic experiments but the aqueous solution of MB was replaced by an aqueous solution of 0.5 mM terephthalic acid and 2 mM NaOH. Samples were extracted every 15 min, and the changes of the fluorescence intensity was detected with a Gangdong F-280 fluorescence spectrophotometer in the range of 350–550 nm at 315 nm of excitation wavelength.

In order to investigate the possible degradation pathway of MB in ZIF-8, impact HD UHR-Q-TOF-MS (Bruker Daltonics) was introduced to detect the byproducts of degradation process. The

analytes were separated by a Thermo Acclaim RSLC 120 C18 (2.2 μm) 120 Å (2.1 × 100 mm) on an Agilent 1290 UHPLC equipped with a DAD detector. Acidified water (0.1% formic acid, v/v) and acidified acetonitrile (0.1% formic acid, v/v) were used as mobile phases A and B respectively. Gradient was programmed as the follows: 0 min, 5% B; 2 min, 5% B; 17 min, 95% B; 30 min, 95% B, and finally, the initial condition was held for 5 min as a re-equilibration step. The flow rate was set at 0.5 mL min^{-1} throughout the gradient. The column temperature was maintained at 30 °C and the injection volume was 5 μL. The UHPLC system was coupled to impact HD UHR-Q-TOF-MS (Bruker Daltonics) equipped with an electrospray ionization source (ESI). Parameters for analysis were set using both positive ionization and negative ionization mode with spectra acquired over a mass range from m/z 50 to 1100, calibrated by external standard HCOONa. The optimum values of the ESI parameters were: capillary, +4500 V, nubilizing gas pressure, 1.8 bar, drying gas flow, 9.0 L min^{-1}; dry gas temperature, 200 °C; collision RF, 150 Vpp; transfer time 70 μs, and pre-pulse storage, 5 μs. The MS data were processed through Data Analysis 4.0 software (Bruker Daltonics, Bermen, Germany) which provided a list of possible elemental formulas by using the Generate Molecular Formula™ editor. The editor uses a CHNO algorithm, which provides standard functionalities such as minimum/maximum elemental range, electron configuration, and ring-plus double bond equivalents, as well as a sophisticated comparison of the theoretical with the measured isotope pattern (mSigma value) for increasing the confidence in the suggested molecular formula.

3. Results and discussion

3.1. Optical band gap

To investigate the conductivity of ZIF-8, the diffuse reflectivity for powder samples was conducted to obtain band gap (E_g). The E_g were confirmed as the intersection point between the energy axis and the line extrapolated from the linear portion of the adsorption edge in a plot of Kubelka–Munk function *F versus* energy *E*. Kubelka–Munk function, $F = (1 - R)^2/2R$,[57] was transformed from the recorded diffuse reflectance data, where R is the diffuse reflectance based on the Kubelka–Munk theory of diffuse reflectance. As shown in Fig. 1, the E_g value assessed from the steep absorption edge for ZIF-8 was 5.16 eV (slightly different to 4.9 eV (ref. 58)), which indicate that ZIF-8 are potential wide gap semiconductive materials.[59,60] Thus, ZIF-8 can be considered as potential photocatalyst to degrade organic pollutants.[61]

3.2. Specific surface area and porous structure of ZIF-8

Specific surface area and porous structure of ZIF-8 were determined by N_2 adsorption–desorption isotherms at 77 K. As shown in Fig. 2a, a type I isotherm which is typical for microporous materials was observed.[62] The Langmuir surface area, Brunauer–Emmett–Teller (BET) surface area and total pore volume of ZIF-8 were calculated to be 1916.5 m^2 g^{-1}, 1799.6 m^2 g^{-1} and 0.6866 cm^3 g^{-1} (calculated from the amount adsorbed at p/p_0 = 0.952), respectively. The pore sizes determined from the N_2-isotherm by means of NLDFT/GCMC-methods using the BELSORP evaluation software, were centered at about 1.4 nm (Fig. 2b). It was reported that the efficiency of adsorbing dye from aqueous solution increase with the increase of surface area of the adsorbing materials.

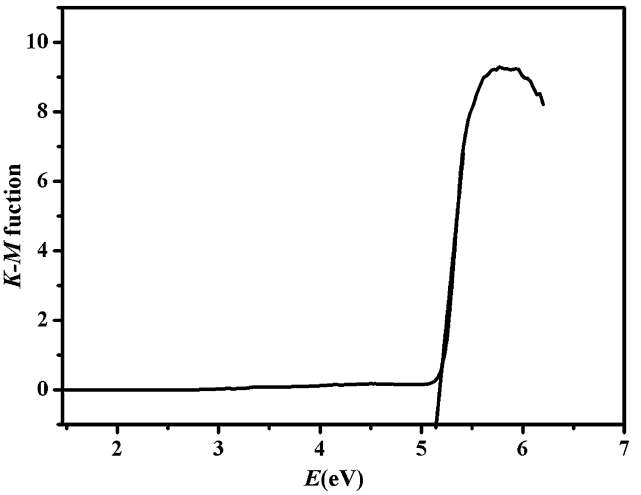

Fig. 1 Kubelka–Munk-transformed diffuse reflectance spectra of ZIF-8.

3.3. Photocatalytic activity of the ZIF-8

The photocatalytic degradation of MB was carried out to evaluate the efficiency of ZIF-8 photocatalyst. In each experiment, the ZIF-8 amount was kept as a constant (0.5 g L^{-1}). The UV-vis absorption spectra of the undecomposed MB in solution during the photocatalytic reaction under UV light irradiation with ZIF-8 was illustrated in Fig. 3a, which indicated that the concentration of MB decreased obviously with the reaction time. Control experiments were conducted to compare the removal efficiencies of MB in two different systems with identical conditions except for in presence of ZIF-8 in dark and absence of ZIF-8 under UV irradiations. Fig. 3b illustrated the changes of MB concentration (C/C_0) with reaction time during these three different reaction systems. After UV light irradiation for 120 min, 20% MB was photocatalytically decomposed in the absence of ZIF-8 photocatalyst, and after 120 min, only 30% MB adsorptive removal was achieved in the presence of ZIF-8 photocatalyst in dark. While *ca.* 82.3% MB was photocatalytically degraded with ZIF-8 as photocatalyst under irradiation of UV light, mainly due to the generation of reactive charge carriers of the excited photoactive ZIF-8. Compared to the previous work reported by other researchers,[63–65] ZIF-8 presented as more active photocatalyst. In addition, the photodegradation of MB dye in ZIF-8 photocatalyst follows pseudo-first-order kinetics model with R^2 = 0.994, as evidenced by the linear plot of $\ln(C/C_0)$ *vs.* reaction time t (Fig. 3c).[56] The pseudo-first-order rate constant for the photocatalytic degradation of MB in ZIF-8 was 1.70 × 10^{-2} min^{-1}.

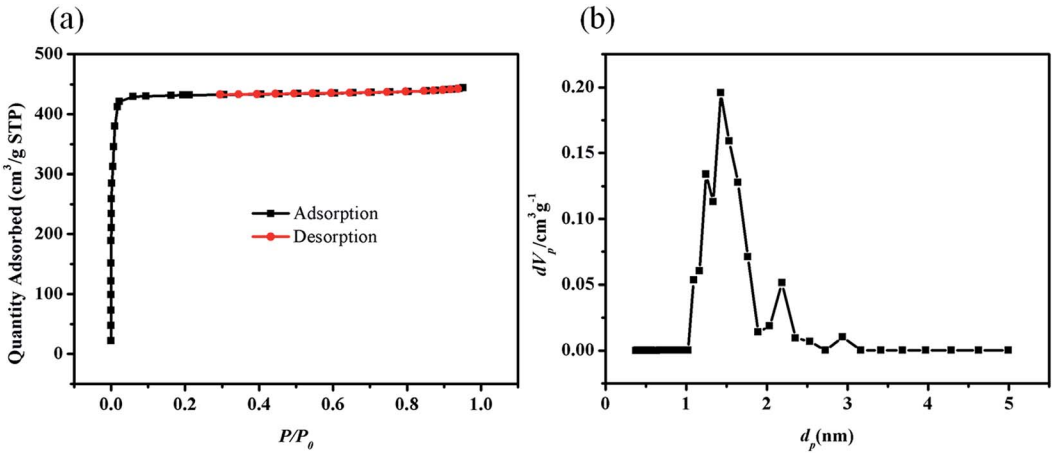

Fig. 2 (a) N_2 adsorption–desorption isotherms of ZIF-8 at 77 K. (b) Micro-pore size distribution of ZIF-8.

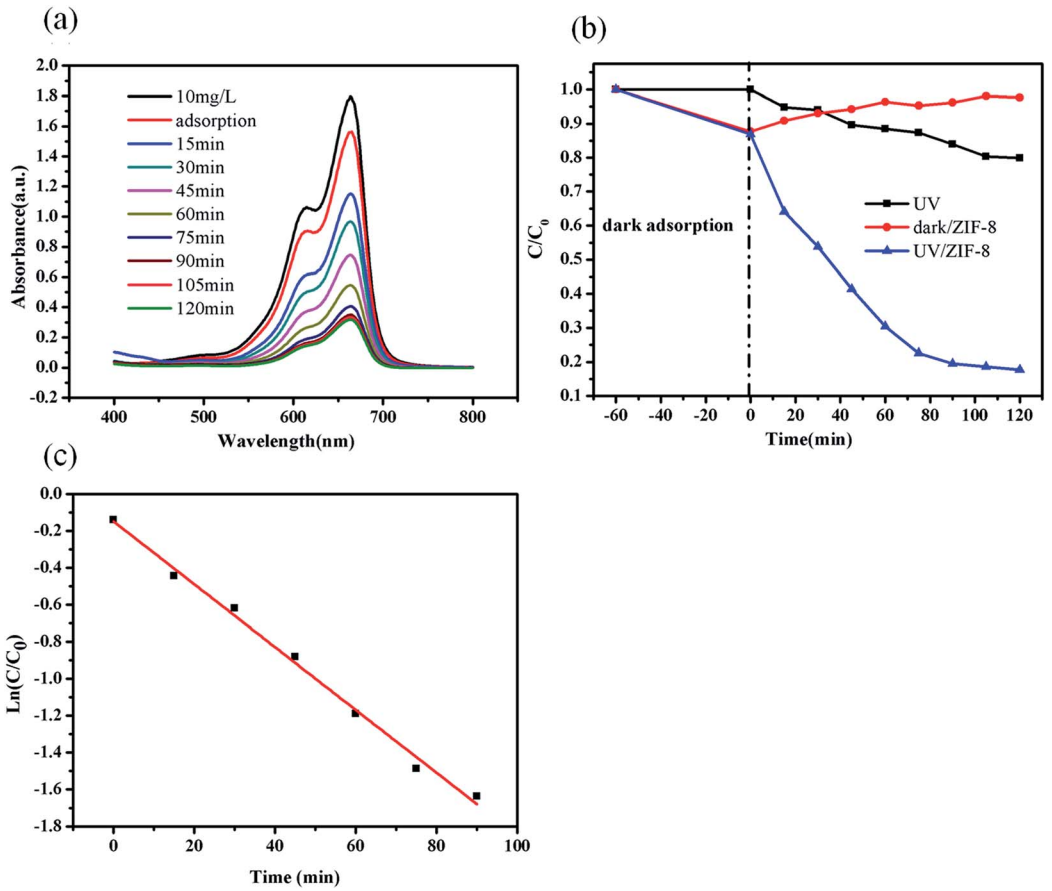

Fig. 3 (a) UV-vis absorption spectra of the MB solution during the decomposition reaction under UV irradiation in the presence of ZIF-8. (b) Degradation of MB under different conditions. (c) Pseudo-first-order kinetics curves of the degradation of MB under UV irradiation in the presence of ZIF-8. Experimental conditions: ZIF-8, 0.5 g L^{-1}; MB, 10 mg L^{-1} and initial pH = 6.

3.3.1. Effect of initial dye concentration. The influence of initial dye concentration on the degradation of MB in ZIF-8/UV light system was also evaluated. As shown in Fig. 4a, the adsorption and degradation efficiencies of MB were found to strongly depend on the initial dye concentration. The degradation efficiency decreased when the concentration of MB increased from 5 to 20 mg L^{-1}, which may be due to the fact that as the initial concentrations of MB increases. The increase of the dye molecules around the active sites resulted in inhibiting the penetration of light to the surface of the catalyst. Hence, the generation of relative amount of $^{\bullet}OH$ and $^{\bullet}O_2^-$ on the surface of the catalyst decreased with the intensity of light and irradiation

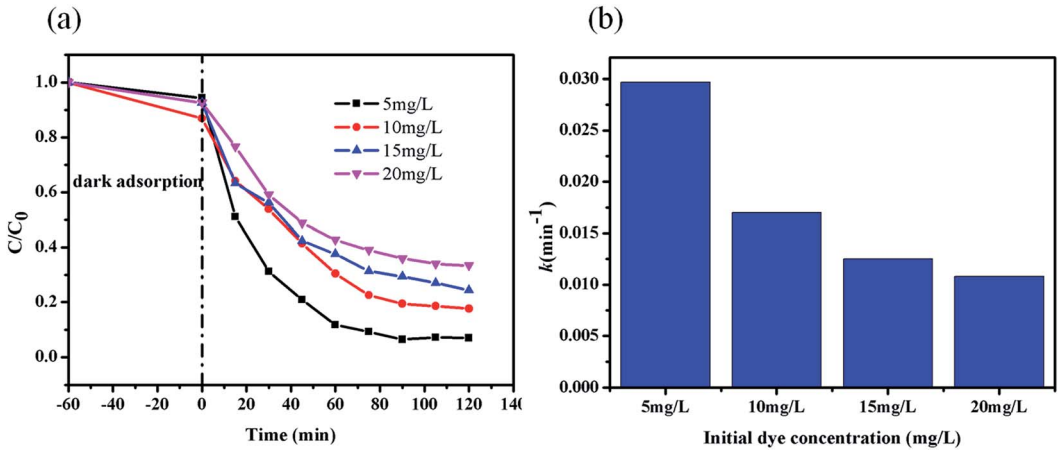

Fig. 4 (a) Effect of initial dye concentration on the degradation of MB. (b) Comparison of the apparent rate constants of the degradation of MB with different initial concentrations. Experimental conditions: ZIF-8, 0.5 g L^{-1} and UV irradiation.

times are constant. The corresponding pseudo-first-order rate constants were 2.97×10^{-2} min^{-1}, 1.70×10^{-2} min^{-1}, 1.25×10^{-2} min^{-1}, and 1.08×10^{-2} min^{-1} for initial MB concentrations of 5 mg L^{-1}, 10 mg L^{-1}, 15 mg L^{-1} and 20 mg L^{-1}, respectively (as illustrated in Fig. 4b).

3.3.2. Effect of initial pH. The pH of the solution was another important parameter which influenced the photocatalytical degradation reactions, since it dictates the surface charge properties of the photocatalyst and size of aggregates formed. In order to determine the effect of initial pH on the adsorption capacity and degradation efficiency of MB, the pH of MB solution was adjusted from 2.0 to 12.0 with HCl or NaOH, and the corresponding pseudo-first-order rate constants were 7×10^{-5} min^{-1}, 0.4×10^{-2} min^{-1}, 1.70×10^{-2} min^{-1}, 1.59×10^{-2} min^{-1}, 1.61×10^{-2} min^{-1} and 3.51×10^{-2} min^{-1}, as illustrated in Fig. 5a and b. The results revealed that the ZIF-8 could work effectively over a wide pH range from 4.0 to 12.0, but no obvious adsorption and degradation appeared when the initial pH was 2.0. When the initial pH of solution increased to 12.0, ZIF-8 showed both high adsorption capacity and degradation efficiency for MB. According to the acid–base equilibrium of MB represented by $MBH^{2+} \leftrightarrow MB + 2H^{+}$, and to its very low pK_a value (less than 1), the removal of MB was due mainly to solubilization of unprotonated form of the dye.[66] The high adsorption capacity for MB may be resulted from electrostatic attraction between the negative charged ZIF-8 adsorbent surface and the positively charged cationic dyes (MB),[67] while the pH of the solution was greater than pH_{pzc} (9.52),[53] much higher than pK_a.[66] As shown in Scheme 2, the increased OH^- concentration may be responsible for the high degradation efficiency for MB as OH^- could neutralize the H^+ generated by photocatalysis.[68] Additionally, the dye adsorption on the adsorbent surface played an essential role in the photodegradation process as higher adsorption should enhance the degradation efficiency.[69] In all, a favourable photocatalyst in strong alkaline environment, is completely different from other traditional photocatalysts.[70]

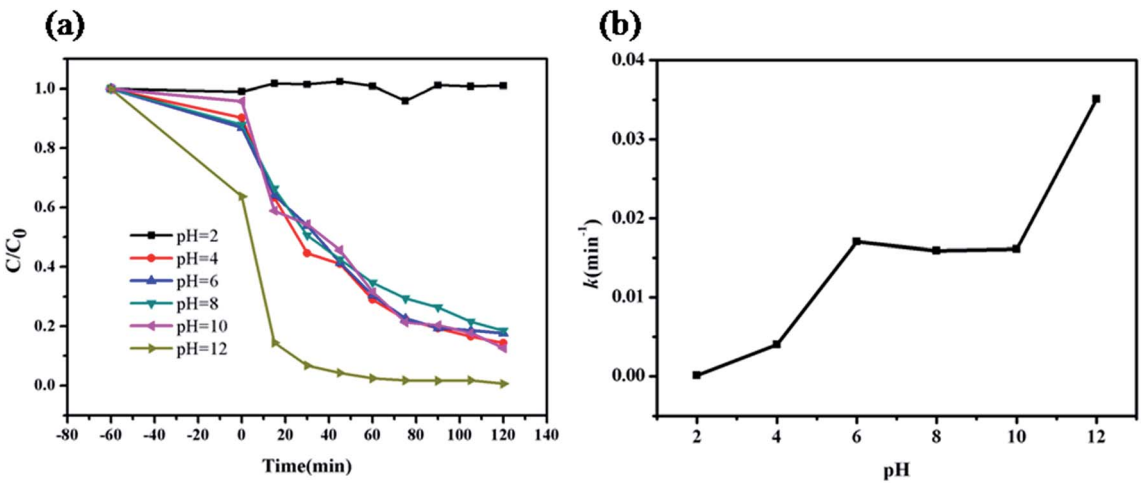

Fig. 5 (a) Effect of initial pH on the degradation of MB. Experimental conditions: ZIF-8, 0.5 g L^{-1}; MB, 10 mg L^{-1} and UV irradiation. (b) The corresponding pseudo-first-order rate constants for system with pH = 2.0–12.0.

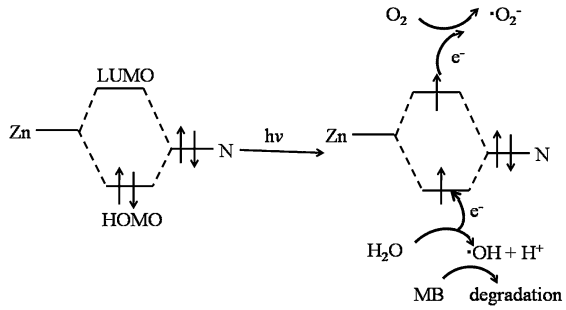

Scheme 2 A simplified model of photocatalytic reaction mechanism of MB on ZIF-8.

3.4. Mechanism and pathway for the MB degradation in ZIF-8

As widely accepted, hydroxyl radicals (˙OH) have been deemed to be the crucial active species during the photocatalytic process. Therefore, the concentration of produced ˙OH radicals, which can be determined by fluorescence intensity, heavily influence the photocatalytic degradation efficiency of dyes in ZIF-8. Fluorescence spectral changes (excitation at 315 nm) observed in the presence of ZIF-8 under the irradiation of UV light, absence of ZIF-8 under the irradiation of UV light and in the presence of ZIF-8 without any light (dark condition) were shown in Fig. 6a–c, respectively. In the case of ZIF-8/UV light system (as shown in Fig. 6a), it was observed that the fluorescence intensity at about 425 nm increases sharply with irradiation time, which indicated that ZIF-8 can favor the formation of ˙OH radicals under UV light irradiation. For comparison, the system under UV light illumination without ZIF-8 and system in presence of ZIF-8 in dark were also investigated under the same conditions. No obvious fluorescence intensity was observed in the presence of ZIF-8 in dark, indicating that no ˙OH radicals were produced. For the system under UV light irradiation without ZIF-8, a gradual increase in fluorescence intensity at about 425 nm was observed with increasing time, suggesting that ˙OH radicals can be generated moderately by UV light irradiation. The strongest fluorescence intensity in the ZIF-8/UV system suggested more ˙OH radicals can be generated, resulted from the existence of synergistic effect by combination of ZIF-8 and UV light irradiation. Obviously, as illustrated in Fig. 6d, the concentration of formed ˙OH radicals increase linearly with the reaction time.

The terminology of HOMO–LUMO gap can be utilized to describe the photocatalytic process of ZIF-8.[26] In the presence of UV light, there is an electron transfer from the highest occupied molecular orbital (HOMO) to the lowest unoccupied molecular orbital (LUMO) in the ZIF-8. The HOMO is mainly contributed

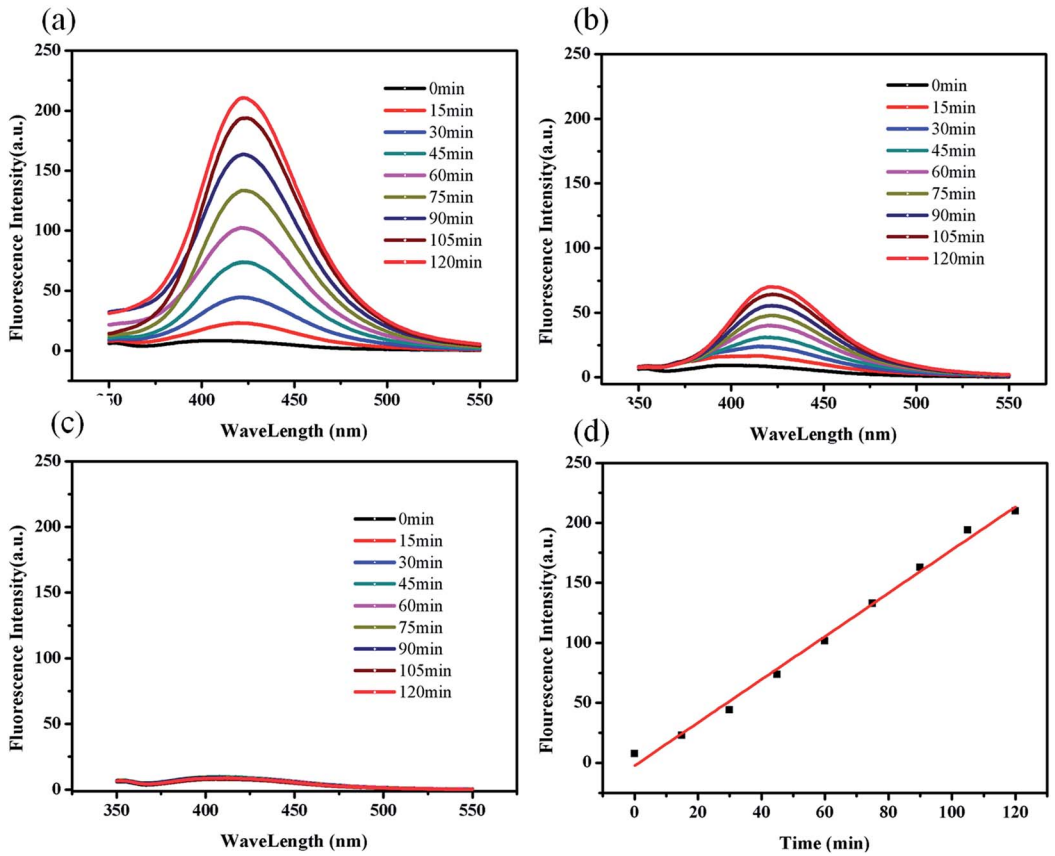

Fig. 6 Fluorescence spectral changes (excitation at 315 nm) observed of: (a) UV light with the presence of ZIF-8; (b) UV light with the absence of ZIF-8; (c) dark with the presence of ZIF-8; (d) Fluorescence intensity changes with UV light irradiation time in the presence of ZIF-8. Experimental conditions: ZIF-8, 0.5 g L^{-1}; terephthalic acid, 0.5 mM; NaOH, 2 mM.

by N 2p bonding orbitals, and the LUMO is mainly contributed by empty Zn orbitals. In general, the electrons of the excited state in the LUMO were easily lost, while the HOMO strongly demanded one electron to return to its stable state. Therefore, one electron was captured from water molecules, which was oxygenated into the ˙OH active species, being confirmed by fluorescence intensity. Then, the ˙OH could decompose MB efficiently to complete the photocatalytic process.

The by-products generated at the end of the degradation process were analysed by Q-TOF-MS equipped with ESI, and identified by comparison with commercial standards and by interpretation of their fragment ions in the mass spectra. Based on the information provided by Q-TOF-MS, a possible pathway can be proposed as Scheme 3, which was similar to the previously reported pathway of MB degradation in TiO_2.[71] Further researches on the final products and intermediates of the photocatalytic degradation, which can favor the description of degradation pathway, should be carried out using more characterization methods, like *in situ* infrared spectra (IR), GC-MS, LC-MS, ion chromatography (IC) and so on.

3.5. Stability of ZIF-8

The crystallographic structures of the as-prepared ZIF-8 samples and used ZIF-8 samples were examined by powder X-ray diffraction (PXRD), as shown in Fig. 7. The results revealed that the well-defined diffraction peaks implied the high crystallinity of the samples, which were also in good agreement with the simulated pattern from CCDC 287180.[52] The almost identical diffraction pattern of as-prepared ZIF-8 samples, used ZIF-8 samples and the simulated patterns illustrated that no structural transformation was happened (see Fig. 7). In order to deeply analyze the molecular structure and identify the functional groups of as-prepared ZIF-8 samples and used ones, the FTIR spectroscopy was recorded, and the results were depicted in Fig. 8. The peaks at 420 cm^{-1} (attributed to the Zn–N stretch mode),[30,72] 1146 and 995 cm^{-1} (assigned to C–N stretch mode),[73] 1584 cm^{-1} (C=N stretch mode) and 2929 cm^{-1} & 3136 cm^{-1} (C–H stretch)[72,73] remained unchanged, indicating that there was no change in the chemical structure of the ZIF-8

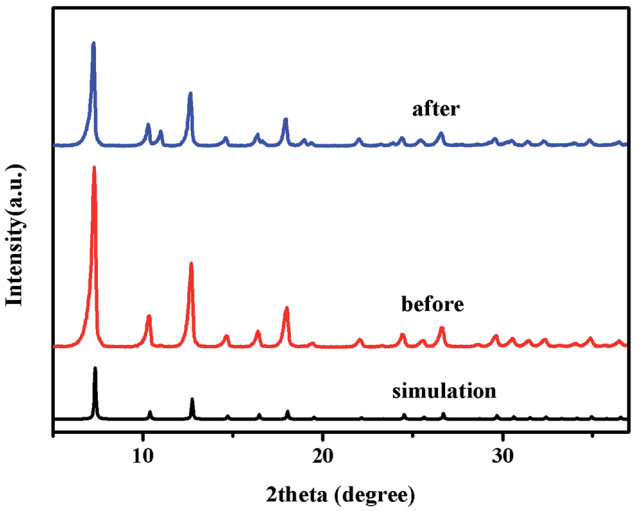

Fig. 7 PXRD patterns of ZIF-8 before and after photocatalytic reaction and the simulated XRD pattern for the ZIF-8 structure created from CIF in ref. 52.

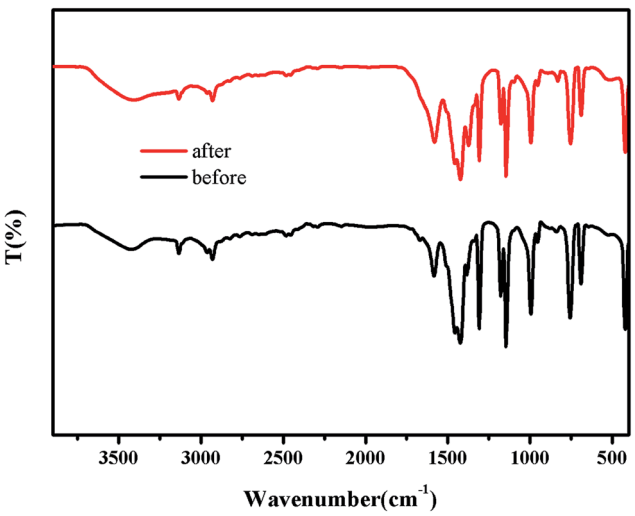

Fig. 8 FTIR spectra of ZIF-8 before and after photocatalytic reaction.

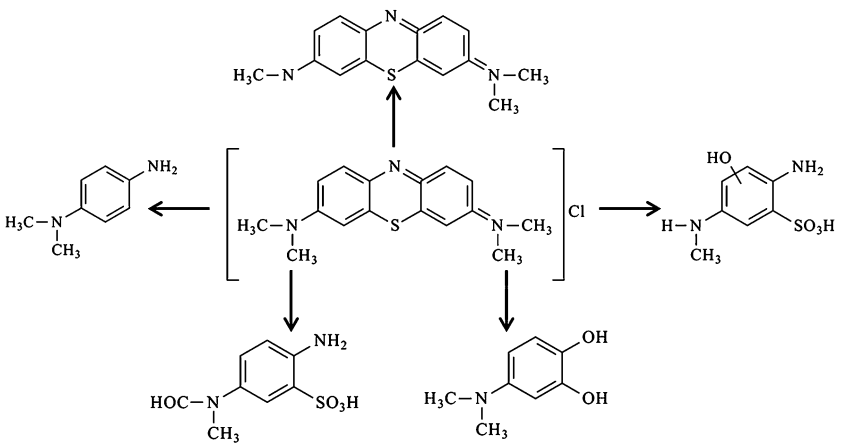

Scheme 3 Proposed photocatalytic degradation pathway of MB in ZIF-8.

samples before and after photocatalytic reactions. These results demonstrated that the ZIF-8 catalyst was stable in aqueous solution, and could be used circularly.

4. Conclusions

ZIF-8 can be considered as an efficient photocatalyst for degradation of methylene blue under UV light irradiation, which was confirmed by the results of detection of hydroxyl radicals (•OH). The photodegradation of MB over ZIF-8 followed pseudo-first-order kinetics, and the rate constant is 1.70×10^{-2} min^{-1} under UV light irradiation. Furthermore, ZIF-8 worked effectively over a wide pH range, and showed both high adsorption capacity and degradation efficiency for MB in strong alkaline environment. Mechanism and pathway for the MB degradation in ZIF-8 were proposed based on the information provided from fluorescence spectra and Q-TOF-MS equipped with ESI. ZIF-8 catalyst was stable in aqueous solution, implying ZIF-8 can be used repeatedly. In all, ZIF-8 can be suggested as potential photocatalyst to degrade organic pollutants.

Acknowledgements

We thank the financial support from the Beijing Natural Science Foundation & Scientific Research Key Program of Beijing Municipal Commission of Education (KZ201410016018), the Training Program Foundation for the Beijing Municipal Excellent Talents (2013D005017000004), the Importation & Development of High-Caliber Talents Project of Beijing Municipal Institutions (CIT&CD201404076), and China Postdoctoral Science of Foundation (2013M540831), National Natural Science Foundation of China (no. 51109002), Open Research Fund Program of Key Laboratory of Urban Stormwater System and Water Environment (Ministry of Education).

References

1 O. M. Yaghi, M. O'Keeffe, N. W. Ockwig, H. K. Chae, M. Eddaoudi and J. Kim, *Nature*, 2003, **423**, 705–714.
2 C. C. Wang, Z. Wang, F. Gu and G. Guo, *J. Mol. Struct.*, 2010, **979**, 92–100.
3 J.-R. Li, J. Sculley and H.-C. Zhou, *Chem. Rev.*, 2011, **112**, 869–932.
4 J.-R. Li and H.-C. Zhou, *Nat. Chem.*, 2010, **2**, 893–898.
5 J.-R. Li, R. J. Kuppler and H.-C. Zhou, *Chem. Soc. Rev.*, 2009, **38**, 1477–1504.
6 X. Duan, R. Song, J. Yu, H. Wang, Y. Cui, Y. Yang, B. Chen and G. Qian, *RSC Adv.*, 2014, **4**, 36419–36424.
7 Y.-X. Tan, Y.-P. He, M. Wang and J. Zhang, *RSC Adv.*, 2014, **4**, 1480–1483.
8 N. L. Rosi, J. Eckert, M. Eddaoudi, D. T. Vodak, J. Kim, M. O'Keeffe and O. M. Yaghi, *Science*, 2003, **300**, 1127–1129.
9 D. J. Collins and H.-C. Zhou, *J. Mater. Chem.*, 2007, **17**, 3154–3160.
10 R. J. Kuppler, D. J. Timmons, Q.-R. Fang, J.-R. Li, T. A. Makal, M. D. Young, D. Yuan, D. Zhao, W. Zhuang and H.-C. Zhou, *Coord. Chem. Rev.*, 2009, **253**, 3042–3066.
11 J. Lee, O. K. Farha, J. Roberts, K. A. Scheidt, S. T. Nguyen and J. T. Hupp, *Chem. Soc. Rev.*, 2009, **38**, 1450–1459.
12 C.-C. Wang, H.-P. Jing and P. Wang, *J. Mol. Struct.*, 2014, **1074**, 92–99.
13 C.-C. Wang, J.-R. Li, X.-L. Lv, Y.-Q. Zhang and G.-S. Guo, *Energ. Environ. Sci.*, 2014, **7**, 2831–2867.
14 Y. Zhang, G. Li, H. Lu, Q. Lv and Z. Sun, *RSC Adv.*, 2014, **4**, 7594–7600.
15 K. Sumida, D. L. Rogow, J. A. Mason, T. M. McDonald, E. D. Bloch, Z. R. Herm, T.-H. Bae and J. R. Long, *Chem. Rev.*, 2011, **112**, 724–781.
16 J.-R. Li, Y. Ma, M. C. McCarthy, J. Sculley, J. Yu, H.-K. Jeong, P. B. Balbuena and H.-C. Zhou, *Coord. Chem. Rev.*, 2011, **255**, 1791–1823.
17 C.-C. Wang, G.-L. Guo and P. Wang, *Transition Met. Chem.*, 2013, **38**, 455–462.
18 C.-C. Wang, H.-Y. Li, G.-L. Guo and P. Wang, *Transition Met. Chem.*, 2013, **38**, 275–282.
19 L.-B. Sun, J.-R. Li, W. Lu, Z.-Y. Gu, Z. Luo and H.-C. Zhou, *J. Am. Chem. Soc.*, 2012, **134**, 15923–15928.
20 H.-C. Zhou, J. R. Long and O. M. Yaghi, *Chem. Rev.*, 2012, **112**, 673–674.
21 J. M. Fang, P. F. Gao and Y. F. Li, *RSC Adv.*, 2014, **4**, 37349–37352.
22 C. G. Silva, A. Corma and H. García, *J. Mater. Chem.*, 2010, **20**, 3141–3156.
23 Y. Horiuchi, T. Toyao, M. Saito, K. Mochizuki, M. Iwata, H. Higashimura, M. Anpo and M. Matsuoka, *J. Phys. Chem. C*, 2012, **116**, 20848–20853.
24 K. G. Laurier, F. Vermoortele, R. Ameloot, D. E. De Vos, J. Hofkens and M. B. Roeffaers, *J. Am. Chem. Soc.*, 2013, **135**, 14488–14491.
25 T. Zhang and W. Lin, *Chem. Soc. Rev.*, 2014, **43**, 5982–5993.
26 M. A. Nasalevich, M. van der Veen, F. Kapteijn and J. Gascon, *CrystEngComm*, 2014, **16**, 4919–4926.
27 S.-L. Li and Q. Xu, *Energy Environ. Sci.*, 2013, **6**, 1656.
28 C.-C. Wang, J. Zhang, P. Wang, H. Wang and H. Yan, *Desalin. Water Treat.*, 2014, DOI: 10.1080/19443994.19442013.19873881.
29 F. Cacho-Bailo, B. Seoane, C. Téllez and J. Coronas, *J. Membr. Sci.*, 2014, **464**, 119–126.
30 S. Gadipelli, W. Travis, W. Zhou and Z. Guo, *Energy Environ. Sci.*, 2014, **7**, 2232–2238.
31 H. Wu, W. Zhou and T. Yildirim, *J. Am. Chem. Soc.*, 2007, **129**, 5314–5315.
32 G. Kumari, K. Jayaramulu, T. K. Maji and C. Narayana, *J. Phys. Chem. A*, 2013, **117**, 11006–11012.
33 Z. Zhang, S. Xian, H. Xi, H. Wang and Z. Li, *Chem. Eng. Sci.*, 2011, **66**, 4878–4888.
34 C. Chen, J. Kim, D. Yang and W.-S. Ahn, *Chem. Eng. J.*, 2011, **168**, 1134–1139.
35 Z. Zhang, S. Xian, Q. Xia, H. Wang, Z. Li and J. Li, *AIChE J.*, 2013, **59**, 2195–2206.
36 H. T. Kwon and H.-K. Jeong, *Chem. Commun.*, 2013, **49**, 3854–3856.
37 K. Díaz, M. López-González, L. F. del Castillo and E. Riande, *J. Membr. Sci.*, 2011, **383**, 206–213.

38 M. C. McCarthy, V. Varela-Guerrero, G. V. Barnett and H.-K. Jeong, *Langmuir*, 2010, **26**, 14636–14641.
39 S. R. Venna and M. A. Carreon, *J. Am. Chem. Soc.*, 2009, **132**, 76–78.
40 H.-L. Jiang, B. Liu, Y.-Q. Lan, K. Kuratani, T. Akita, H. Shioyama, F. Zong and Q. Xu, *J. Am. Chem. Soc.*, 2011, **133**, 11854–11857.
41 H. B. Wu, S. Wei, L. Zhang, R. Xu, H. H. Hng and X. W. D. Lou, *Chem.–Eur. J.*, 2013, **19**, 10804–10808.
42 C. Chizallet, S. Lazare, D. Bazer-Bachi, F. Bonnier, V. Lecocq, E. Soyer, A.-A. Quoineaud and N. Bats, *J. Am. Chem. Soc.*, 2010, **132**, 12365–12377.
43 U. P. Tran, K. K. Le and N. T. Phan, *ACS Catal.*, 2011, **1**, 120–127.
44 R.-Q. Zhong, R.-Q. Zou, T. Nakagawa, M. Janicke, T. A. Semelsberger, A. K. Burrell and R. E. Del Sesto, *Inorg. Chem.*, 2012, **51**, 2728–2730.
45 S. A. Moggach, T. D. Bennett and A. K. Cheetham, *Angew. Chem.*, 2009, **121**, 7221–7223.
46 K. Zhang, R. P. Lively, C. Zhang, W. J. Koros and R. R. Chance, *J. Phys. Chem. C*, 2013, **117**, 7214–7225.
47 J. A. Gee, J. Chung, S. Nair and D. S. Sholl, *J. Phys. Chem. C*, 2013, **117**, 3169–3176.
48 Y.-N. Wu, M. Zhou, B. Zhang, B. Wu, J. Li, J. Qiao, X. Guan and F. Li, *Nanoscale*, 2014, **6**, 1105–1112.
49 G. Lu and J. T. Hupp, *J. Am. Chem. Soc.*, 2010, **132**, 7832–7833.
50 F. Yan, Z.-Y. Liu, J.-L. Chen, X.-Y. Sun, X.-J. Li, M.-X. Su, B. Li and B. Di, *RSC Adv.*, 2014, **4**, 33047–33054.
51 I. B. Vasconcelos, T. G. da Silva, G. C. Militão, T. A. Soares, N. M. Rodrigues, M. O. Rodrigues, N. B. da Costa, R. O. Freire and S. A. Junior, *RSC Adv.*, 2012, **2**, 9437–9442.
52 X. C. Huang, Y. Y. Lin, J. P. Zhang and X. M. Chen, *Angew. Chem., Int. Ed. Engl.*, 2006, **45**, 1557–1559.
53 W. S. Wan Ngah, L. C. Teong, R. H. Toh and M. A. K. M. Hanafiah, *Chem. Eng. J.*, 2013, **223**, 231–238.
54 X. Fang, G. Mark and C. von Sonntag, *Ultrason. Sonochem.*, 1996, **3**, 57–63.
55 W. Jiang, J. A. Joens, D. D. Dionysiou and K. E. O'Shea, *J. Photochem. Photobiol., A*, 2013, **262**, 7–13.
56 L. Ai, C. Zhang, L. Li and J. Jiang, *Appl. Catal., B*, 2014, **148–149**, 191–200.
57 Y. Gong, T. Wu and J. Lin, *CrystEngComm*, 2012, **14**, 3727–3736.
58 F. Wang, Z. S. Liu, H. Yang, Y. X. Tan and J. Zhang, *Angew. Chem., Int. Ed.*, 2011, **50**, 450–453.
59 H.-S. Liu, Y.-Q. Lan and S.-L. Li, *Cryst. Growth Des.*, 2010, **10**, 5221–5226.
60 J. Guo, J.-F. Ma, B. Liu, W.-Q. Kan and J. Yang, *Cryst. Growth Des.*, 2011, **11**, 3609–3621.
61 B. Liu, J. Yang, G. C. Yang and J. F. Ma, *Inorg. Chem.*, 2013, **52**, 84–94.
62 H. Reinsch, M. Krüger, J. Wack, J. Senker, F. Salles, G. Maurin and N. Stock, *Microporous Mesoporous Mater.*, 2012, **157**, 50–55.
63 X. Wang, N. Han, H. Lin, J. Luan, A. Tian and D. Liu, *Inorg. Chem. Commun.*, 2014, **42**, 10–14.
64 X.-L. Wang, Z.-H. Chang, H.-Y. Lin, G.-C. Liu, C. Xu, J. Luan, A.-X. Tian and J.-W. Zhang, *Inorg. Chim. Acta*, 2014, **413**, 16–22.
65 J. Guo, J. Yang, Y.-Y. Liu and J.-F. Ma, *Inorg. Chim. Acta*, 2013, **400**, 51–58.
66 N. Zaghbani, A. Hafiane and M. Dhahbi, *Sep. Purif. Technol.*, 2007, **55**, 117–124.
67 J. L. Gong, B. Wang, G. M. Zeng, C. P. Yang, C. G. Niu, Q. Y. Niu, W. J. Zhou and Y. Liang, *J. Hazard. Mater.*, 2009, **164**, 1517–1522.
68 L.-L. Wen, F. Wang, J. Feng, K.-L. Lv, C.-G. Wang and D.-F. Li, *Cryst. Growth Des.*, 2009, **9**, 3581–3589.
69 J. Zhao, C. Chen and W. Ma, *Top. Catal.*, 2005, **35**, 269–278.
70 M. N. Chong, B. Jin, C. W. Chow and C. Saint, *Water Res.*, 2010, **44**, 2997–3027.
71 A. Houas, H. Lachheb, M. Ksibi, E. Elaloui, C. Guillard and J.-M. Herrmann, *Appl. Catal., B*, 2001, **31**, 145–157.
72 T. Zhang, X. Zhang, X. Yan, L. Kong, G. Zhang, H. Liu, J. Qiu and K. L. Yeung, *Chem. Eng. J.*, 2013, **228**, 398–404.
73 M. J. C. Ordoñez, K. J. Balkus, J. P. Ferraris and I. H. Musselman, *J. Membr. Sci.*, 2010, **361**, 28–37.

